UNIVERSITY *of* York

This is a repository copy of *Temperature dependence of spin-transport properties and spin torque in a magnetic nanostructure*.

White Rose Research Online URL for this paper:
https://eprints.whiterose.ac.uk/id/eprint/170191/

Version: Published Version

Article:

White Rose
university consortium
Universities of Leeds, Sheffield & York

eprints@whiterose.ac.uk
https://eprints.whiterose.ac.uk/

Temperature dependence of spin-transport properties and spin torque in a magnetic nanostructure

W. Boonruesi,[1] J. Chureemart,[1] R. W. Chantrell,[2] and P. Chureemart [1,*]

[1]*Department of Physics, Mahasarakham University, Mahasarakham 44150, Thailand*
[2]*Department of Physics, University of York, York YO10 5DD, United Kingdom*

The study and understanding of spin-transport mechanisms including thermal fluctuation are required for the development and design of spintronic devices. In this paper, we present an approach to investigate the temperature dependence of spin-transport behavior within the magnetic structure by using the generalized spin accumulation model. The temperature affects not only the magnetization orientation, but also the spin-transport properties. Its effect on transport parameters can be taken into account by considering the spin-dependent resistivity at any finite temperature. This leads to the calculation of temperature-dependent spin-transport parameters and eventually allows the calculation of the thermal effects on spin accumulation, spin current, and spin torque. It is observed that increasing temperature is likely to decrease the value of key transport parameters relevant to the magnitude of spin torque. This study demonstrates the importance of thermal effects on spin-transport behavior which needs to be considered for spin-transfer torque based device design with high performance.

I. INTRODUCTION

The emergence of spintronics has had a rapid impact on the development of future data storage technology. Exploiting electron spin in addition to the electron charge to store and transport information offers the possibility to improve the performance of devices with nonvolatility, high operation speed, and low power consumption [1–5]. It is evidently shown that the electron spin plays a key role in the transport properties, in particular for the spin-transfer torque (STT)-based devices with dimensions much less than the spin-diffusion length of the material such as spin-transfer torque magnetic random access memory (STT-MRAM), racetrack memory, magnetic tunneling junction (MTJ), and read sensors for magnetic recording [6–10]. The understanding of the STT phenomenon and spin-transport behavior in magnetic structures is of great importance since it opens novel possibilities to manipulate and control the magnetization for write and read processes in magnetic memory devices. The physics underlying STT can be described in terms of a spin accumulation via the *s-d* exchange interaction. The mechanism starts with injecting the spin current into the magnetic structure. As a result of the exchange interaction between spin current and the local magnetization, the spin-polarized current then flows through the magnetic layer and exerts a torque on the magnetization, which tends to reorient in the direction of the spin-polarized current [11,12].

For the write and read processes of STT-based devices, the spin torque property is used to write the desired magnetic state of the data bits in the memory array. The charge current is injected into the magnetic structure to control the direction of magnetization to store the data bits in the write process

and, at a lower current density, to detect the readback signal during reading. The injected current increases the temperature and generates the additional heat in the devices, the so-called Joule heating effect [13–15]. Therefore, understanding the effect of temperature on the operation of devices is crucial since it provides insight into the underlying physics and also the mechanism of STT in the presence of thermal fluctuation. It has been reported that the temperature effect arising from the injected current density leads to the reduction of STT and eventually increases the difficulty for write and read processes [16]. Importantly, a high temperature caused by Joule heating could cause thermal instability of data bits. For the efficient development and design of STT-based devices, it is important to understand the spin-transport property, particularly including the effect of temperature.

The spin-transport behavior in magnetic structures can be described by using a generalized spin-accumulation model based on the drift-diffusion equation [17–23]. To understand the physics and mechanism of STT including temperature effects, the temperature dependence of spin-transport parameters is required as important information for spin-accumulation calculations. However, it has not been investigated intensively. Some transport parameters, i.e., the spin-diffusion length, spin polarization, and resistivity as a function of temperature, have been experimentally studied via the spin-relaxation mechanism [24–29], but other key parameters contributing to spin-transport behavior still remain to be investigated. For a promising step towards potential STT-based device design, in this work, we investigate spin-transport behavior in the magnetic structure in the presence of thermal fluctuation via the physical quantity of spin accumulation, spin current, and STT. As is well known, the thermal fluctuation affects not only the spin-transport behavior, but also the magnetization profile. Here, the atomistic model implemented in the open-source VAMPIRE software package

_____
*phanwadee.c@msu.ac.th

[30] is employed to investigate the magnetization profile of the magnetic structure at nonzero temperature. Meanwhile, the spin-accumulation model is used to present a qualitative description of the STT acting on the magnetization. In this computational study, the investigation is presented in two stages. First, we calculate the temperature dependence of spin-transport parameters by using the approach based on the two-channel model [26] through the spin-dependent resistivity of the material. Subsequently, the influence of temperature on the spin-transfer torque occurring in the magnetic structure is considered.

II. MODEL DESCRIPTION

To investigate the spin-transfer torque including the effect of temperature, there are two necessary parts to determine. The first part is the calculation of the temperature dependence of transport parameters, which will be used for the second part providing the detail of STT determination in the presence of temperature.

A. Temperature dependence of transport parameters

In order to characterize the spin-dependent transport parameters at any finite temperature, the spin-dependent resistivity of the ferromagnetic 3d transition material is first considered in the following form [26,31,32]:

$$\rho_i = \rho_{0i} + \alpha T + A_i T^2, \tag{1}$$

where ρ_{0i} is the low-temperature resistivity accounting for the spin-flip scattering, α and A_i are empirical constants, and i represents the spin-up ($\uparrow$), spin-down ($\downarrow$), and spin-mixing ($\uparrow\downarrow$) resistivities. However, it is generally found that the coefficient α is relatively small, for example, lower than 0.01×10^{-11} Ω cm K^{-1} for Co. The second term in the right-hand side of the above equation can be negligible. Subsequently, the conductivities of up- and down-spin channels can be expressed in terms of the spin-dependent resistivity given by

$$\sigma_{\uparrow(\downarrow)} = \frac{\rho_{\downarrow(\uparrow)} + 2\rho_{\uparrow\downarrow}}{\rho_{\uparrow}\rho_{\downarrow} + \rho_{\uparrow\downarrow}(\rho_{\uparrow} + \rho_{\downarrow})}. \tag{2}$$

Subsequently, the key spin-transport parameters at any given temperature used to describe the spin-transport behavior within a magnetic structure are considered directly from the spin-dependent conductivities. The spin-polarization parameters of conductivity (β) as a function of temperature can be first calculated from the following relationship with the assumption that the coefficient A, indicating the strength of the temperature effect on the spin-flip scattering, is fixed as $A = A_{\uparrow} = A_{\downarrow} = A_{\uparrow\downarrow}$:

$$\beta(T) = \frac{\sigma_{\uparrow} - \sigma_{\downarrow}}{\sigma_{\uparrow} + \sigma_{\downarrow}} = \frac{\rho_{0\downarrow} - \rho_{0\uparrow}}{\rho_{0\downarrow} + \rho_{0\uparrow} + 4\rho_{0\uparrow\downarrow} + 6AT^2}, \tag{3}$$

and the spin-polarization parameter of diffusion constant (β') can be expressed in terms of the conductivity from the Einstein relation, $\sigma = e^2 N(E_F)D$, given by

$$\beta'(T) = \frac{D_{\uparrow} - D_{\downarrow}}{D_{\uparrow} + D_{\downarrow}} = \frac{N_{\downarrow}\sigma_{\uparrow} - N_{\uparrow}\sigma_{\downarrow}}{N_{\downarrow}\sigma_{\uparrow} + N_{\uparrow}\sigma_{\downarrow}}$$

$$= \frac{\beta(T) - \beta''}{1 - \beta(T)\beta''}$$

$$= \frac{(\rho_{0\downarrow} - \rho_{0\uparrow}) - \beta''(\rho_{0\downarrow} + \rho_{0\uparrow} + 4\rho_{0\uparrow\downarrow} + 6AT^2)}{(\rho_{0\downarrow} + \rho_{0\uparrow} + 4\rho_{0\uparrow\downarrow} + 6AT^2) - \beta''(\rho_{0\downarrow} - \rho_{0\uparrow})}, \tag{4}$$

with $\beta'' = \frac{N_{\uparrow}(E_F) - N_{\downarrow}(E_F)}{N_{\uparrow}(E_F) + N_{\downarrow}(E_F)}$, where $N_{\uparrow(\downarrow)}(E_F)$ is the density of state for up (down) spin at the Fermi energy level.

The spin-diffusion length is an important length scale over which the spin of the electrons diffuses between spin-flip scattering events. It is defined as $\lambda_{sdl} = \lambda_{sf}\sqrt{1 - \beta\tilde{\beta}}$ and $\lambda_{sf} = \sqrt{2D_0\tau_{sf}}$, with D_0 being the diffusion constant. A number of experimental studies show that the spin-diffusion length is linearly proportional to $1/\rho$ as seen in Eq. (5). This relationship indicates the main contribution from the Elliott-Yafet (EY) scattering to the spin-relaxation mechanism [26,28,33],

$$\lambda_{sdl} = \frac{C}{\rho} = C(\sigma_{\uparrow} + \sigma_{\downarrow}), \tag{5}$$

where C is an empirical constant obtained from experiment. The spin-diffusion length can be expressed in terms of spin-dependent resistivity and temperature by putting Eqs. (1) and (2) into (5); therefore we obtain

$$\lambda_{sdl}(T) = C\left[\frac{\rho_{0\downarrow} + \rho_{0\uparrow} + 4\rho_{0\uparrow\downarrow} + 6AT^2}{B + 2AT^2(\rho_{0\uparrow} + \rho_{0\downarrow} + \rho_{0\uparrow\downarrow}) + 3A^2T^4}\right], \tag{6}$$

where $B = \rho_{0\downarrow}\rho_{0\uparrow} + \rho_{0\uparrow\downarrow}(\rho_{0\downarrow} + \rho_{0\uparrow})$.

So far, several experimental studies have focused mostly on determining the temperature dependence of the spin-diffusion length and spin polarization of lateral spin valve structures [26,28,33,34]. However, to investigate the temperature dependence of spin-transfer torque (STT) arising from the s-d exchange interaction between the transverse spin accumulation and local magnetization, it is important to consider the diffusion constant (D_0) as a function of temperature since the magnitude of STT decays over the length scale, $\lambda_J = \sqrt{2\hbar D_0/J}$, associated with the diffusion constant [35]. According to the EY mechanism, the spin-relaxation time (τ_{sf}) is proportional to the conductivity (σ) [34,36–39], written as

$$\tau_{sf} = \frac{\tau_p}{\epsilon} = \kappa\sigma, \tag{7}$$

with the coefficient $\kappa = m_e/ne^2\epsilon$, where τ_p is the momentum relaxation time, ϵ is the spin-flip probability occurring at momentum scattering events, and n is the conduction electron density. Thus the temperature dependence of the diffusion constant can be represented as follows:

$$D_0 = \frac{\lambda_{sdl}^2}{2\kappa\sigma(1 - \beta\tilde{\beta})}. \tag{8}$$

The spin-transport parameters as a function of temperature can be evaluated by using Eqs. (1)–(8) as described above. Subsequently, the calculation of spin-transfer torque acting on the magnetization in a magnetic structure at any given temperature is achieved by using a model of spin accumulation, described in the next section, in which the polarized spin current interacts with the local magnetization via the s-d exchange interaction.

B. Spin-transfer torque (STT)

The STT arising from the s-d exchange interaction between the nonequilibrium conduction electrons and the local magnetization can be qualitatively described by the generalized spin-accumulation model based on drift-diffusion equations [23,35,40]. The spin accumulation is defined as the difference of the spin-up and spin-down density of states (DOS) and its general solution in the rotated coordinate system $\hat{\mathbf{b}}_1$, $\hat{\mathbf{b}}_2$, and $\hat{\mathbf{b}}_3$ consists of longitudinal ($\mathbf{m}_\parallel$) and transverse ($\mathbf{m}_\perp$) components which are parallel and perpendicular to the local magnetization expressed in the following form:

$$\mathbf{m}_\parallel(x) = [m_\parallel(\infty) + [m_\parallel(0) - m_\parallel(\infty)]e^{-x/\lambda_{\text{sdl}}}]\hat{\mathbf{b}}_1,$$
$$\mathbf{m}_{\perp,2}(x) = 2e^{-k_1 x}[u\cos(k_2 x) - v\sin(k_2 x)]\hat{\mathbf{b}}_2, \quad (9)$$
$$\mathbf{m}_{\perp,3}(x) = 2e^{-k_1 x}[u\sin(k_2 x) + v\cos(k_2 x)]\hat{\mathbf{b}}_3,$$

with

$$(k_1 \pm ik_2) = \sqrt{\lambda_{\text{trans}}^{-2} \pm i\lambda_J^{-2}}.$$

The transverse length scale (λ_{trans}) including the dephasing effect [19,35] is defined as $\lambda_{\text{trans}}^{-2} = \lambda_\phi^{-2} + \lambda_{\text{sf}}^{-2}$, with λ_ϕ the spin dephasing length. The unknown coefficients $m_\parallel(0)$, u, and v can be calculated by imposing the boundary condition of the continuity of the spin current. The spin current ($\mathbf{j}_m$), which is temperature and position dependent, can be written in terms of the transport parameters, the charge current density (j_e), and the gradient of spin accumulation as follows:

$$\mathbf{j}_m = \beta j_e \mathbf{M} - 2D_0\left[\frac{\partial \mathbf{m}}{\partial x} - \beta\beta'\mathbf{M}\left(\mathbf{M} \cdot \frac{\partial \mathbf{m}}{\partial x}\right)\right], \quad (10)$$

where $\mathbf{M}$ is the unit vector of the magnetization and x is the direction of the injected current.

The mechanism of STT involving the s-d exchange interaction can be theoretically described by considering the spin current carried by the conduction electrons into the magnetic structure. The STT acts on the spin current to adiabatically align in the direction of the local magnetization. According to the conservation of angular momentum, a reaction torque proportional to the spin current density is simultaneously created on the local magnetization. The STT (τ_{STT}), naturally including the adiabatic (AST, τ_{AST}) and nonadiabatic spin torques (NAST, τ_{NAST}), can be quantitatively described in the following form:

$$\tau_{\text{STT}} = \tau_{\text{AST}} + \tau_{\text{NAST}} = \frac{\partial \mathbf{j}_m}{\partial x}$$
$$= -(J/\hbar)(\mathbf{m} \times \mathbf{M}) - (J/\hbar)\frac{\ell_L}{\ell_\perp}[\mathbf{M} \times (\mathbf{m} \times \mathbf{M})]$$
$$- \frac{2D_0}{\lambda_{\text{sf}}^2}\mathbf{m}$$
$$= \frac{2D_0}{\lambda_J^2}(\mathbf{M} \times \mathbf{m}) + \frac{2D_0}{\lambda_\phi^2}[\mathbf{M} \times (\mathbf{M} \times \mathbf{m})] - \frac{2D_0}{\lambda_{\text{sf}}^2}\mathbf{m}, \quad (11)$$

where $\lambda_J = \sqrt{2\hbar D_0/J}$ and the spin dephasing length $\lambda_\phi = \sqrt{2\hbar D_0 \ell_\perp/(J\ell_L)}$. Parameters ℓ_L and $\ell_\perp$ are the spin precession length and spin coherence length [19], respectively.

Next the STT arising from the transverse component of spin accumulation ($\mathbf{m}_\perp$) is decomposed into two components:

The in-plane torque (AST) and the fieldlike torque or the out-of-plane torque (NAST). They can be derived in the rotated basis system where the AST and NAST are along the directions of $\hat{\mathbf{b}}_2$ and $\hat{\mathbf{b}}_3$, respectively [23]. We substitute $\mathbf{M} = \hat{\mathbf{b}}_1$ and $\mathbf{m} = m_{\perp,2}\hat{\mathbf{b}}_2 + m_{\perp,3}\hat{\mathbf{b}}_3$ into the above equation; therefore, we obtain

$$\tau_{\text{STT}} = \frac{2D_0}{\lambda_J^2}(-m_{\perp,3}\hat{\mathbf{b}}_2 + m_{\perp,2}\hat{\mathbf{b}}_3) + \frac{2D_0}{\lambda_\phi^2}(-m_{\perp,2}\hat{\mathbf{b}}_2 - m_{\perp,3}\hat{\mathbf{b}}_3)$$
$$- \frac{2D_0}{\lambda_{\text{sf}}^2}(+m_{\perp,2}\hat{\mathbf{b}}_2 + m_{\perp,3}\hat{\mathbf{b}}_3)$$
$$= 2D_0\left[\left(-\frac{m_{\perp,2}}{\lambda_{\text{trans}}^2} - \frac{m_{\perp,3}}{\lambda_J^2}\right)\hat{\mathbf{b}}_2 + \left(\frac{m_{\perp,2}}{\lambda_J^2} + \frac{m_{\perp,3}}{\lambda_{\text{trans}}^2}\right)\hat{\mathbf{b}}_3\right], \quad (12)$$

where the first and second terms of the above equation represent AST and NAST as follows:

$$\tau_{\text{AST}} = -\frac{2D_0}{\lambda_J^2\lambda_{\text{trans}}^2}\left(\lambda_J^2 m_{\perp,2} + \lambda_{\text{trans}}^2 m_{\perp,3}\right)\hat{\mathbf{b}}_2,$$
$$\tau_{\text{NAST}} = \frac{2D_0}{\lambda_J^2\lambda_{\text{trans}}^2}\left(\lambda_{\text{trans}}^2 m_{\perp,2} + \lambda_J^2 m_{\perp,3}\right)\hat{\mathbf{b}}_3. \quad (13)$$

As clearly seen in Eq. (13), STT strongly depends on the transport parameters and decays over the length scale of λ_J and λ_{trans} associated with D_0. Therefore, it is important to consider these parameters correctly for the appropriate design of STT-based devices.

III. RESULTS AND DISCUSSION

The aim of this paper is to understand the temperature dependence of STT acting on magnetization in a magnetic structure and to get insight into the physical description of the STT mechanism behind the operation of devices. STT domain-wall (STT-DW) based memory offers a new possibility to increase the data storage capacity for today's information-based society [41]. In this section, we therefore study the enhancement of STT in the DW structure formed in the the Co thin film at any finite temperature. The transport parameters of Co as a function of temperature are first calculated by using the formalism in Eqs. (1) to (8), and they will be subsequently used for the calculation of STT.

A. Spin-transport parameters including temperature effect

The temperature dependence of the electrical resistivity in Eq. (1) plays a key role in the determination of other transport parameters. According to an experimental study of Co in Ref. [31], the coefficient α is relatively small and negligible. Therefore, the spin-dependent resistivity of Co can be expressed in the following form: $\rho_i = \rho_{0i} + A_i T^2$. The empirical constant $A_\uparrow = A_\downarrow = A_{\uparrow\downarrow}$ is estimated to be $1.6 \times 10^{-7}\,\mu\Omega\,\text{m}\,\text{K}^{-2}$. In addition, the values of the low-temperature resistivity for spin up, spin down, and spin mixing of Co are taken from experiments [42,43]: $\rho_{0\uparrow} = 0.041\,\mu\Omega\,\text{m}$, $\rho_{0\downarrow} = 0.11\,\mu\Omega\,\text{m}$, and $\rho_{0\uparrow\downarrow} = 0$, respectively. Based on these parameters, the calculated spin-dependent resistivity is shown in Fig. 1(a), where the calculated total
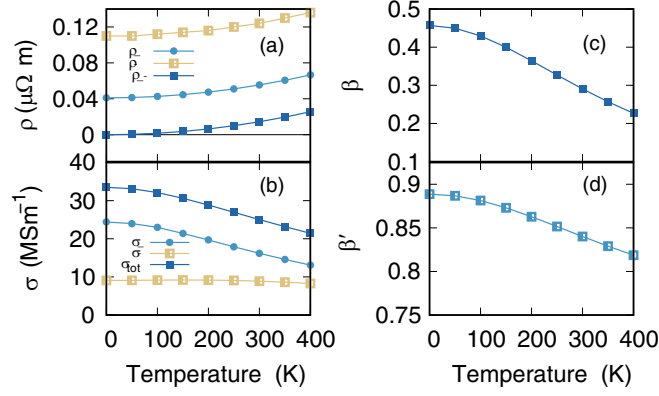
FIG. 1. Temperature dependence of (a) spin-dependent resistivity, (b) spin-dependent conductivity, (c) spin-polarization parameters for the conductivity, and (d) spin-polarization parameters for the diffusion constant of Co calculated directly from Eqs. (1)–(4) by using parameters from experiments in Refs. [31,42,43].

resistivity at 4.2 K of $\rho_{4.2K} = 0.03\ \mu\Omega$ m is close to prior studies [33,43,44].

Subsequently, the temperature dependence of conductivity, spin-polarization parameters for conductivity, and diffusion can be obtained as shown in Figs. 1(b)–1(d). $\sigma_\uparrow$ is significantly decreased by temperature due to the spin-flip scattering [32,45], whereas $\sigma_\downarrow$ is relatively unchanged. The behavior of total conductivity becomes dominated by $\sigma_\uparrow$. The reduction of spin-dependent conductivities results in the decrease of spin-polarization parameters β and β', as expected [32]. In addition, the value of the spin-polarization parameter of conductivity is predicted to have a value of $\beta = 0.457$ at low temperature, which is in good agreement with experimental studies [33,46]. This confirms the validity of the parameters used in this paper.

The spin-diffusion length and diffusion constant of Co as a function of temperature are next considered by using the experimental values of λ_{sdl} and the resistivity at any given temperature, as shown in Table I. The results show the inverse proportionality of the spin-diffusion length to the resistivity. The coefficient $C = 2.09$ f Ω m^2 in Eq. (5) was evaluated from a linear fit to the results of λ_{sdl} versus $1/\rho$ obtained from the literature in Refs. [42,47], as illustrated in Fig. 2 (inset). The empirical constant from the best fit is used to determine the temperature-dependent λ_{sdl} by substitution into Eq. (6). At low temperature, the spin-diffusion length varies slowly with a more rapid decrease at high temperature. The thermal effect gives rise to a high probability of spin flipping within the material, which finally leads to the reduction of the spin-diffusion length. Our simulated results are similar to

TABLE I. Spin-diffusion length and conductivity of Co at any given temperature [42,47].

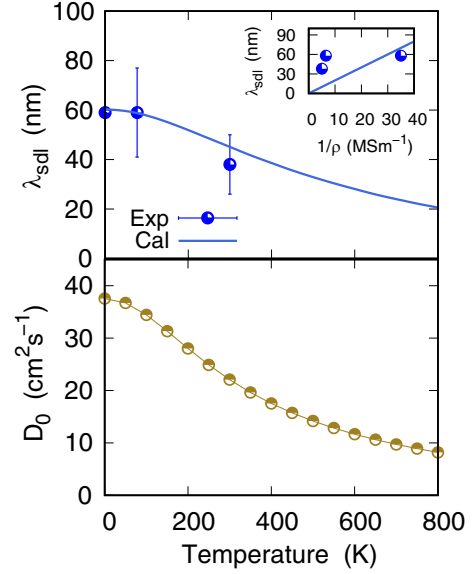| Temperature (K)	λ_{sdl} (nm)	ρ (nΩ m)
0	60	30
77	59 ± 18	160
300	38 ± 12	210

FIG. 2. Spin-diffusion length and diffusion constant as a function of temperature: An inset shows the linear dependence of the spin-diffusion length and $1/\rho$ extracted from previous experiments [42,47]. The solid line (inset) is the best fit to the experimental data.

previous reports [37,39,47,48]. The diffusion constant is next considered due to its importance in relation to the magnitude of STT. The temperature dependence of D_0 can be obtained by substituting the calculated σ, β, β', and λ_{sdl} into Eq. (8) with the constant $\kappa = 3 \times 10^{-20}\ \Omega$ ms [42]. As clearly seen in Fig. 2, there is a strong decrease of the diffusion constant with increasing temperature. This indicates the fast change of the spin direction stimulated by thermal fluctuation [34].

These results emphasize the significant effect of temperature on the spin-transport parameters. To describe the spin-transport behavior in a magnetic structure, in the following section, the temperature-dependent transport parameter will be used for the calculation of spin accumulation, spin current, and STT acting on a domain wall in Co. This study demonstrates the importance of applying the empirical process outlined here to materials for spintronic device design since these devices are operated at finite temperature.

B. STT calculation in the presence of thermal effect

The thermal fluctuation strongly influences the magnetic and transport properties. Here we choose to investigate the temperature dependence of the STT on a domain-wall (DW) structure in a Co thin film using an atomistic model based on the VAMPIRE software package [30]. The combination of the atomistic spin model and the temperature-dependent spin accumulation allows the calculation of the corresponding temperature dependence of the spin-transfer torque acting on the domain wall. We first evaluate the temperature dependence of the magnetization of Co using the Monte Carlo method implemented in the VAMPIRE software package [30], as depicted in Fig. 3 where the Curie temperature is approximately $T_c = 1400$ K. The parameters for Co are a uniaxial anisotropy constant of $k_u = 6.69 \times 10^{-24}$ J/atom, exchange energy $J_{ij} =$
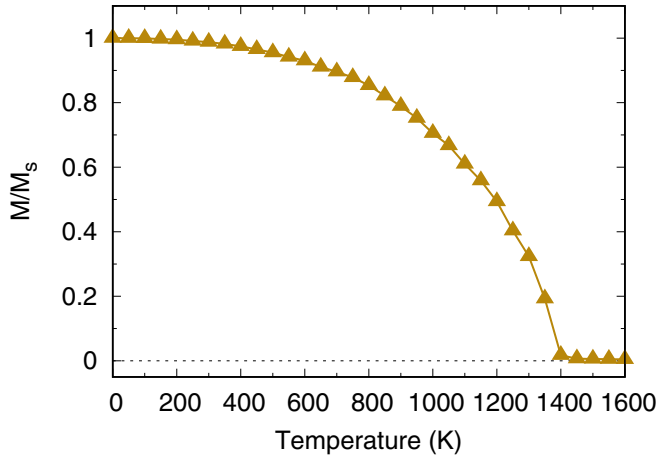
FIG. 3. Temperature-dependent magnetization of Co obtained from atomistic simulation.

6.064×10^{-21} J/link, and the atomic spin moment of $\mu_s = 1.72\mu_b$.

The DW structure in a Co thin film with the dimensions of $70 \times 35 \times 1.75$ nm^3 at different temperatures ranging from 0 to 1200 K is next investigated by employing the atomistic spin dynamic simulations. The dynamical behavior of each local spin (S_i) in the magnetic system can be described by the stochastic Landau-Lifshitz-Gilbert equation given by

$$\frac{\partial \mathbf{S}_i}{\partial t} = -\frac{\gamma}{(1+\alpha^2)}(\mathbf{S}_i \times \mathbf{B}_{\text{eff},i}) - \frac{\gamma\alpha}{(1+\alpha^2)}[\mathbf{S}_i \times (\mathbf{S}_i \times \mathbf{B}_{\text{eff},i})],$$

$$(14)$$

with the local field given by

$$\mathbf{B}_{\text{eff},i} = \sum_{i \neq j} \frac{J_{ij}\mathbf{S}_j}{|\mu_s|} + \frac{2k_u}{|\mu_s|}(\mathbf{S}_i \cdot \mathbf{e})\mathbf{e} + \mathbf{B}_{\text{dip},k} + \mathbf{B}_{\text{th},i}, \quad (15)$$

where $\mathbf{S}_i$ is the normalized spin moment at site i, γ is the modulus of the gyromagnetic ratio, α is the damping constant, and $\mathbf{B}_{\text{eff},i}$ denotes the effective field of local spin i. The constant J_{ij} is the nearest-neighbor spin exchange energy between spin sites i and j, k_u is the uniaxial anisotropy constant, $\mathbf{e}$ is the unit vector of the easy axis, and $|\mu_s|$ is the magnitude of the spin moment.

The first two terms in Eq. (15) represent the contribution of the exchange interaction field and anisotropy field, respectively. Due to the expensive computation time, the inclusion of a demagnetization field is considered separately using the macrocell approach [23,30] under the assumption that the demagnetizing field of macrocell k containing spin i is constant over the cell given by

$$\mathbf{B}_{\text{dip},k} = \frac{\mu_0}{4\pi} \sum_{l \neq k} \left[\frac{3(\boldsymbol{\mu}_l \cdot \hat{\mathbf{r}}_{kl})\hat{\mathbf{r}}_{kl} - \boldsymbol{\mu}_l}{|r_{kl}|^3} \right] \quad (16)$$

and

$$\boldsymbol{\mu}_l = \mu_s \sum_{i=1}^{n_{\text{atom}}} \mathbf{S}_i, \quad (17)$$

where $\boldsymbol{\mu}_l$ is the vector of the magnetic moment in the macrocell site l, μ_0 is the permeability of free space, V is the
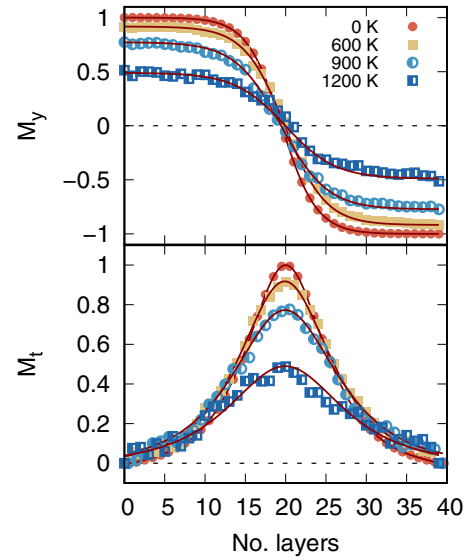

FIG. 4. Schematic representation of the easy axis (M_y) and transverse (M_t) components of magnetization in domain-wall formation with different temperatures obtained from atomistic simulation: The distance between layers is 1.75 nm. Lines provide a guide to the eye.

volume of the macrocell, r_{kl} is the distance and $\hat{\mathbf{r}}_{kl}$ is the corresponding unit vector between macrocell sites k and l, and n_{atom} is the number of atoms in each macrocell.

Finally, the contribution of a random thermal field acting on the spin site i is introduced into the atomistic model by a Gaussian distribution $\boldsymbol{\Gamma}$ with a mean of zero as follows:

$$\mathbf{B}_{\text{th},i} = \boldsymbol{\Gamma}\sqrt{\frac{2\alpha k_B T}{\gamma \mu_s \Delta t}}, \quad (18)$$

where k_B is the Boltzmann constant, T is the system temperature in Kelvin, and Δt is the time step.

In order to quantify the DW profile, the spin accumulation, and the spin torque, the system is discretized into macrocells $1.75 \times 1.75 \times 1.75$ nm^3 in size. The equilibrium domain-wall structure at any finite temperature can be obtained by pinning the magnetization at the boundaries of the film along the easy axis direction, $\pm y$, to force a domain wall into the film. The spin dynamics simulation is performed as described above. Figure 4 demonstrates the easy axis and transverse components of the magnetization in a DW formed in a Co thin film. The thermal fluctuation results in the decrease of magnetization and a Bloch wall is observed at high temperature. Next, the domain-wall width (δ) at any temperature can be evaluated from the easy axis or y component of the magnetization in DW obtained from simulation, as seen in Fig. 5. The results clearly show an increase in the domain-wall width with temperature consistent with previous work [49]. This can be explained since the DW width depends on the anisotropy and exchange stiffness, $\delta = \pi\sqrt{A/K}$, associated with temperature. Since A scales with M^2 and for Co the uniaxial anisotropy scales with M^3 and with increasing temperature, the wall width δ diverges as M^{-1}.

Finally, we investigate the spin accumulation, spin current, and spin torque in the DW structure as a function of temperature. The simulated magnetization profile in the DW and
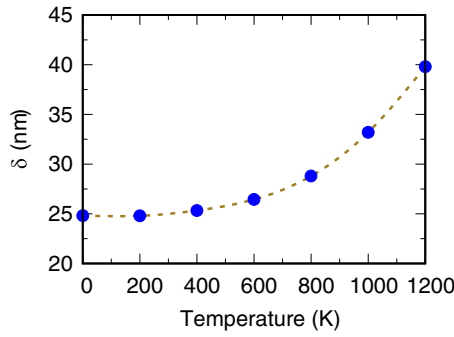
FIG. 5. Temperature dependence of the domain-wall width.

calculated transport parameters presented earlier are used to determine the spin current, spin accumulation, and spin torque acting on the magnetization within the DW. The investigation starts with injecting a charge current density of $5 \times 10^{11}\,\mathrm{A/m^2}$ into the DW structure along the x direction. For clarity, the spatial variation of spin accumulation and spin current within the DW at different temperatures is best presented in the basis coordinate system showing the longitudinal and transverse components. The procedure works by a sliding system into many thin layers ($i = 0, 1, 2, \ldots, n$). Subsequently, Eqs. (9) and (10) are applied to each thin layer of the system to determine the spin accumulation and spin current at any position. It is worth noting that the previous layer (i-1) acts as the pinned layer for the considered layer (i) [22]. In general, the spin accumulation and spin current are likely to reach the equilibrium value in the direction of magnetization. It is interesting that both spin accumulation and spin current easily develop towards the direction of the local magnetization at high temperature, as seen in Figs. 6(a) and 6(c). It is also important to consider the magnitude of the transverse or out-of-plane component of the spin accumulation inducing a spin torque acting on the local magnetization. It physically indicates the degree of spin mistracking, which is the inability of conduction electrons to follow the magnetization. The results shown in Figs. 6(b) and 6(d) clearly suggest that the spin mistracking is strongly dependent on temperature. It can be

seen that the transverse spin accumulation decreases rapidly with temperature above 300 K.

The spin accumulation strongly depends on the gradient of magnetization between layers and relaxes towards the direction of magnetization with the characteristic length scale of the spin-diffusion length. The temperature affects not only the orientation of magnetization within the DW, but also the transport parameters, especially the spin-diffusion length and the spin-polarization parameters. Increasing the temperature results in a decrease of the anisotropy constant, leading to a wider DW and a reduction in the spin-diffusion length. At high temperature, the spins of conduction electrons easily flow across the DW with small gradient of magnetization and relax to the equilibrium value with small deviation due to the strong interaction between the conduction electrons and the magnetization. In turn, for a narrow DW and large spin-diffusion length at low temperature, as seen in Figs. 5 and 2, there is a large deviation of the longitudinal spin accumulation ($\mathbf{m}_\parallel$) from the equilibrium value across the DW. As a consequence of the inability of the spin accumulation to follow the magnetization at low temperature, the transverse spin accumulation arising from the spin mistracking can be clearly observed.

To gain insight into the effect of temperature on the spin-transport behavior, the spin torque consisting of adiabatic (AST) and nonadiabatic spin torque (NAST) is discussed next. Physically, STT originates from the transverse spin accumulation and its magnitude is related to the phase difference between the magnetization and spin accumulation [40]. Therefore, the result of spin accumulation depicted in Fig. 6
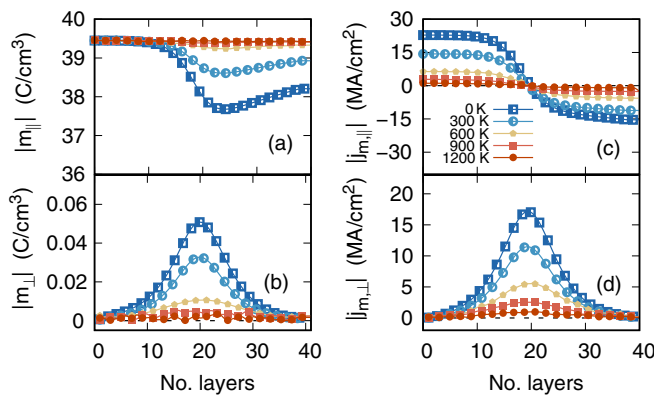

FIG. 6. The spatial variation of the (a) longitudinal and (b) transverse spin accumulation, and the (c) longitudinal and (d) transverse component of the spin current with various temperatures ranging from 0 to 1200 K.
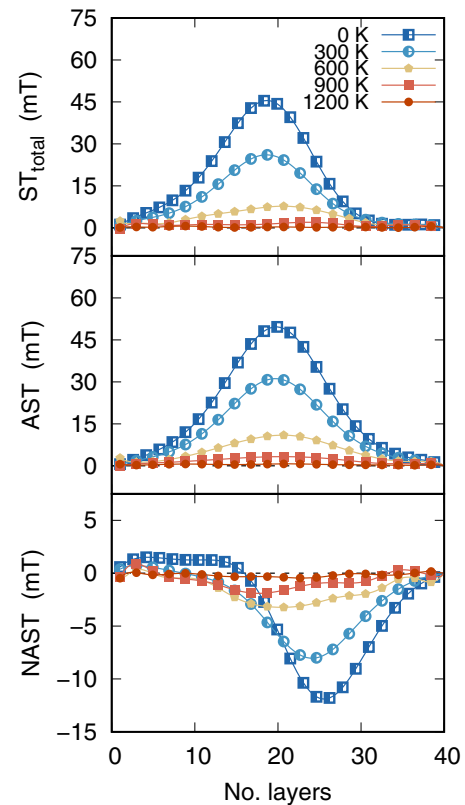

FIG. 7. The spin-transfer torque acting on the local magnetization within the domain wall.

can be used to describe the spin torque exerted on the DW. Figure 7 shows the total spin torque and the contribution of AST and NAST on the spatially continuous magnetization in domain walls at different temperatures. For all temperatures, the magnitude of the STT follows the direction of magnetization within the domain wall. The conduction electron spins follow the direction of the local magnetization, resulting in a predominantly adiabatic process dominated by the AST. The total STT mainly arises from the AST orienting in the plane of magnetization of the domain wall and the maximum AST appears at the center of the wall due to the strong gradient of magnetization. On the other hand, the NAST arising from the deviation of conduction electrons from the adiabatic process is relatively small. Its magnitude is a few times smaller than that of AST, as illustrated in Fig. 7; however, it may give rise to the out-of-plane component of magnetization in dynamic processes. Obviously, the highest spin torque at the center of the DW is observed since the transverse spin accumulation is mostly absorbed in this position. In addition, the results demonstrate that the temperature plays a crucial role in the spin-transport behavior. The thermal effect on AST and NAST is larger at low temperature due not only to the larger magnetization gradient in a narrow DW, but also to a long spin-diffusion length. The results of this study provide evidence that increasing the temperature results in a decrease in spin-diffusion length and an increase in DW width, which eventually leads to a decrease in spin-torque magnitude. The proposed model described here can form an important basis for the understanding of the thermal influence on spin-transport behavior and implications for the STT-based device design.

IV. CONCLUSION

In conclusion, the calculation of the temperature dependence of spin-transport parameters, which is required for the potential applications based on STT, is demonstrated here. The transport parameters as a function of temperature can be determined via the spin-dependent resistivity of the material. The spin-polarization parameter, the spin-diffusion length, and the diffusion constant are decreased with increasing temperature, in agreement with experiments. As an exemplar, the calculated transport parameters for Co are taken into the spin-accumulation model to investigate the thermal effect on spin-transport behavior within a DW in a Co thin film. STT arises from the transverse component of spin accumulation, which is generally small, but it significantly induces the spin torque in the system. Interestingly, the results also show that thermal fluctuations have a significant effect on the magnitude of STT. This is due to the fact that the spin accumulation is associated with not only the relative orientation of magnetization, but also the transport parameters which are temperature dependent. These investigations are of fundamental interest and give useful insight into the influence of temperature on the spin-transport behavior to understand and control the magnetization in devices.

[1] S. A. Wolf, A. Y. Chtchelkanova, and D. M. Treger, IBM J. Res. Dev. **50**, 101 (2006).

[2] S. Bhatti, R. Sbiaa, A. Hirohata, H. Ohno, S. Fukami, and S. Piramanayagam, Mater. Today **20**, 530 (2017).

[3] E. E. Fullerton and J. R. Childress, Proc. IEEE **104**, 1787 (2016).

[4] T. Endoh and H. Honjo, J. Low Power Electron. Appl. **8**, 44 (2018).

[5] G. Finocchio, M. D. Ventra, K. Y. Camsari, K. Everschor-Sitte, P. K. Amiri, and Z. Zeng, The promise of spintronics for unconventional computing, arXiv:1910.07176.

[6] M. Hosomi, H. Yamagishi, T. Yamamoto, K. Bessho, Y. Higo, K. Yamane, H. Yamada, M. Shoji, H. Hachino, C. Fukumoto *et al.*, in *IEEE International Electron Devices Meeting*, IEDM Technical Digest (IEEE, Piscataway, New Jersey, 2005), pp. 459–462.

[7] W. J. Gallagher and S. S. Parkin, IBM J. Res. Dev. **50**, 5 (2006).

[8] R. Wood, J. Magn. Magn. Mater. **321**, 555 (2009).

[9] S. S. Parkin, M. Hayashi, and L. Thomas, Science **320**, 190 (2008).

[10] Y. Huai, AAPPS Bull. **18**, 33 (2008).

[11] L. Berger, Phys. Rev. B **54**, 9353 (1996).

[12] J. Slonczewski, J. Magn. Magn. Mater. **159**, L1 (1996).

[13] G. E. Bauer, E. Saitoh, and B. J. Van Wees, Nat. Mater. **11**, 391 (2012).

[14] H. Fangohr, D. S. Chernyshenko, M. Franchin, T. Fischbacher, and G. Meier, Phys. Rev. B **84**, 054437 (2011).

[15] E. Ramos, C. López, J. Akerman, M. Muñoz, and J. L. Prieto, Phys. Rev. B **91**, 214404 (2015).

[16] N. Strelkov, A. Chavent, A. Timopheev, R. C. Sousa, I. L. Prejbeanu, L. D. Buda-Prejbeanu, and B. Dieny, Phys. Rev. B **98**, 214410 (2018).

[17] S. Zhang, P. M. Levy, and A. Fert, Phys. Rev. Lett. **88**, 236601 (2002).

[18] K.-J. Lee, M. D. Stiles, H.-W. Lee, J.-H. Moon, K.-W. Kim, and S.-W. Lee, Phys. Rep. **531**, 89 (2013).

[19] C. Petitjean, D. Luc, and X. Waintal, Phys. Rev. Lett. **109**, 117204 (2012).

[20] C. Abert, M. Ruggeri, F. Bruckner, C. Vogler, G. Hrkac, D. Praetorius, and D. Suess, Sci. Rep. **5**, 14855 (2015).

[21] P. Chureemart, R. Cuadrado, I. D'Amico, and R. W. Chantrell, Phys. Rev. B **87**, 195310 (2013).

[22] P. Chureemart, I. D'Amico, and R. W. Chantrell, J. Phys.: Condens. Matter **27**, 146004 (2015).

[23] P. Chureemart, R. F. L. Evans, I. D'Amico, and R. W. Chantrell, Phys. Rev. B **92**, 054434 (2015).

[24] T. Kimura, T. Sato, and Y. Otani, Phys. Rev. Lett. **100**, 066602 (2008).

[25] Y. Ando, K. Kasahara, S. Yamada, Y. Maeda, K. Masaki, Y. Hoshi, K. Sawano, M. Miyao, and K. Hamaya, Phys. Rev. B **85**, 035320 (2012).

[26] E. Villamor, M. Isasa, L. E. Hueso, and F. Casanova, Phys. Rev. B **88**, 184411 (2013).

[27] Ikhtiar, S. Kasai, Y. K. Takahashi, T. Furubayashi, S. Mitani, and K. Hono, Appl. Phys. Lett. **108**, 062401 (2016).

[28] E. Sagasta, Y. Omori, M. Isasa, Y. Otani, L. E. Hueso, and F. Casanova, Appl. Phys. Lett. **111**, 082407 (2017).

[29] G. Zahnd, L. Vila, V. T. Pham, M. Cosset-Cheneau, W. Lim, A. Brenac, P. Laczkowski, A. Marty, and J. P. Attané, Phys. Rev. B **98**, 174414 (2018).

[30] R. F. L. Evans, W. J. Fan, P. Chureemart, T. A. Ostler, M. O. A. Ellis, and R. W. Chantrell, J. Phys.: Condens. Matter **26**, 103202 (2014).

[31] M. Isshiki, Y. Fukuda, and K. Igaki, J. Phys. F: Met. Phys. **14**, 3007 (1984).

[32] M. Zhu, C. L. Dennis, and R. D. McMichael, Phys. Rev. B **81**, 140407(R) (2010).

[33] H. Y. T. Nguyen, W. Pratt, Jr., and J. Bass, J. Magn. Magn. Mater. **361**, 30 (2014).

[34] G. Mihajlović, J. E. Pearson, S. D. Bader, and A. Hoffmann, Phys. Rev. Lett. **104**, 237202 (2010).

[35] N. Saenphum, J. Chureemart, R. Chantrell, and P. Chureemart, J. Magn. Magn. Mater. **484**, 238 (2019).

[36] R. J. Elliott, Phys. Rev. **96**, 266 (1954).

[37] S. R. Marmion, M. Ali, M. McLaren, D. A. Williams, and B. J. Hickey, Phys. Rev. B **89**, 220404(R) (2014).

[38] C. Guite and V. Venkataraman, Appl. Phys. Lett. **101**, 252404 (2012).

[39] J. T. Batley, M. C. Rosamond, M. Ali, E. H. Linfield, G. Burnell, and B. J. Hickey, Phys. Rev. B **92**, 220420(R) (2015).

[40] P. Chureemart, R. F. L. Evans, and R. W. Chantrell, Phys. Rev. B **83**, 184416 (2011).

[41] H. Mohammed, S. A. Risi, T. L. Jin, J. Kosel, S. N. Piramanayagam, and R. Sbiaa, Appl. Phys. Lett. **116**, 032402 (2020).

[42] M. R. Sears and W. M. Saslow, Phys. Rev. B **85**, 014404 (2012).

[43] M. D. Stiles, J. Xiao, and A. Zangwill, Phys. Rev. B **69**, 054408 (2004).

[44] J. Bass and W. Pratt, J. Magn. Magn. Mater. **200**, 274 (1999).

[45] A. C. Gossard *et al.*, *Advanced Epitaxy for Future Electronics, Optics, and Quantum Physics: Seventh Lecture International Science Lecture Series* (Washington, D.C., 2000), Vol. 7.

[46] S. V. Karthik, T. M. Nakatani, A. Rajanikanth, Y. K. Takahashi, and K. Hono, J. Appl. Phys. **105**, 07C916 (2009).

[47] J. Bass and W. P. Pratt, Jr., J. Phys.: Condens. Matter **19**, 183201 (2007).

[48] T. O'Donnell, N. Wang, S. Kulkarni, R. Meere, F. M. Rhen, S. Roy, and S. O'Mathuna, J. Magn. Magn. Mater. **322**, 1690 (2010).

[49] R. Moreno, R. F. L. Evans, S. Khmelevskyi, M. C. Muñoz, R. W. Chantrell, and O. Chubykalo-Fesenko, Phys. Rev. B **94**, 104433 (2016).